Magnetotransport properties in a compensated semimetal gray arsenic

Lingxiao Zhao,[1] Qiunan Xu,[1] Xinmin Wang,[1] Junbao He,[1] Jing Li,[1] Huaixin Yang,[1] Yujia Long,[1] Dong Chen,[1] Hui Liang,[1] Chunhong Li,[1] Mianqi Xue,[1] Jianqi Li,[1,2,3] Zhian Ren,[1,2,3] Li Lu,[1,2,3] Hongmin Weng,[1,2] Zhong Fang,[1,2,3] Xi Dai,[1,2,3,*] and Genfu Chen[1,2,3,†]

[1]*Institute of Physics and Beijing National Laboratory for Condensed Matter Physics, Chinese Academy of Sciences, Beijing 100190, China*

[2]*School of Physical Sciences, University of Chinese Academy of Sciences, Beijing 100190, China*

[3]*Collaborative Innovation Center of Quantum Matter, Beijing 100190, China*

(Received 19 October 2016; revised manuscript received 19 January 2017; published 10 March 2017)

We report the observation of an extremely large magnetoresistance (up to 15 000 000% at 1.8 K in a magnetic field of 9 T) in a simple chemical element, gray arsenic, in which the magnitude of the magnetoresistance increases as approximately the square of the magnetic field strength without any signs of saturation. The Hall-effect study confirms that gray arsenic is a nearly perfect "compensated semimetal," with a small concentration of very mobile carriers, which lead to an extremely large magnetoresistance. The analysis of Shubnikov–de Haas oscillations reveals a nontrivial π Berry phase, a strong signature of Dirac fermions with three-dimensional dispersion. Furthermore, in the presence of parallel magnetic and electric fields, a weak antilocalization effect and a pronounced negative longitudinal magnetoresistance, which may be linked to novel topological states, are also observed. These findings which uncover the material's basis in gray arsenic not only open avenues in spintronics and magnetic sensor applications but also provide more platforms to study topological materials.

DOI: 10.1103/PhysRevB.95.115119

The "giant" or "colossal" magnetoresistance has emerged over the past three decades as an area of increasing interest to both fundamental and applied science, which has recently been enriched by very recent developments on the topologically ordered materials [1–7]. These exotic phases induced by strong spin-orbit coupling are known to exist mainly in pnictide and selenide compounds, especially in arsenic-based materials [4–7].

Gray arsenic (α-As), the most common type of arsenic, adopts a layered structure, consisting of many ruffled, six-member buckled rings [as shown in Fig. 1(a)] [8]. Similar to graphite, the bonds between layers are comparatively weak and so it can easily be intercalated and exfoliated. Recent theoretical calculation [9] suggests that thin films of α-As display a significant band gap depending sensitively on the number of layers or in-layer strain, in contrast to the bulk material which is more usually described as a semimetal, implying that this material has a huge potential in electronic applications. However, unlike the well-studied semimetal of bismuth, which is also belong to the group VA, there are few experimental work performed on either bulk or thin film of arsenic to date, except for the comprehensive study of Fermi surface (FS) topology by the de Haas–van Alphen (dHvA) effect and Shubnikov–de Haas (SdH) effect [10–14].

The magnetic field has been considered to be one of the most powerful tools in studying the electronic properties of semimetals [4–7]. Based on the magnetotransport measurements, many exotic transport behaviors, such as extremely large magnetoresistance, ultrahigh carrier mobility, anomalous Berry phase, and/or negative longitudinal magnetoresistance have been observed. In this work, we performed systematic magnetotransport studies on the α-As single crystal in the temperature range from 1.8 K to room temperature at magnetic fields up to 9 T. We observed an ultrahigh carrier mobility ($\mu_h \approx 9.35 \times 10^5\ \mathrm{cm^2\,V^{-1}\,s^{-1}}$, $\mu_e \approx 2.4 \times 10^5\ \mathrm{cm^2\,V^{-1}\,s^{-1}}$ at 1.8 K) and an extremely large quadratic field-dependent magnetoresistance (MR = 15 000 000%, T = 1.8 K and B = 9 T). Both the observed MR and Hall resistance behavior could be qualitatively explained by the semiclassical two-band model, in which the high mobility is responsible for the rapid increase of resistivity with applied magnetic fields as described by $\rho_{xx} \sim (\mu B)^2$, while the nearly perfect balance of electron and hole populations would likely prevent the saturation of MR in sufficiently high magnetic fields [4]. Further analysis of the SdH oscillations reveals the existence of a nontrivial π Berry phase. Notably, in the presence of parallel magnetic and electric fields, a weak antilocalization (WAL) effect and a pronounced negative longitudinal MR are observed. Our observations yield a strong signature of three-dimensional (3D) Dirac or Weyl fermions' characters as detected in other topological semimetals [5–7], but this scenario seems unlikely in α-As since the first-principles calculations and angle-resolved photoemission spectroscopy (ARPES) experiment have shown that it is a topological insulator [TI] [15]. Further research would be helpful to better understand the exotic magnetotransport properties in α-As in the near future.

High-quality single crystals of α-As were grown using a modified Bridgman technique. Initially, the purchased As lumps (99.9999%) were purified by the sublimation method as reported in Ref. [16]. The purified As was then loaded into a tapered quartz tube and was sealed under high vacuum. The sealed tube was placed vertically inside a muffle furnace, and was heated to 820 °C at a rate of 40 °C/h and held for duration of 10 h before cooling slowly to 500 °C at 1 °C/h. Then the furnace is cooled down to room temperature at 10 °C/h. The obtained crystals were characterized by x-ray diffraction (XRD) using a PANalytical diffractometer (Cu $K\alpha_1$ radiation, λ = 1.540 51 Å). The XRD pattern of a single crystal reveals three peaks that could be indexed as 00l reflections in a crystal

*daix@iphy.ac.cn
†gfchen@iphy.ac.cn

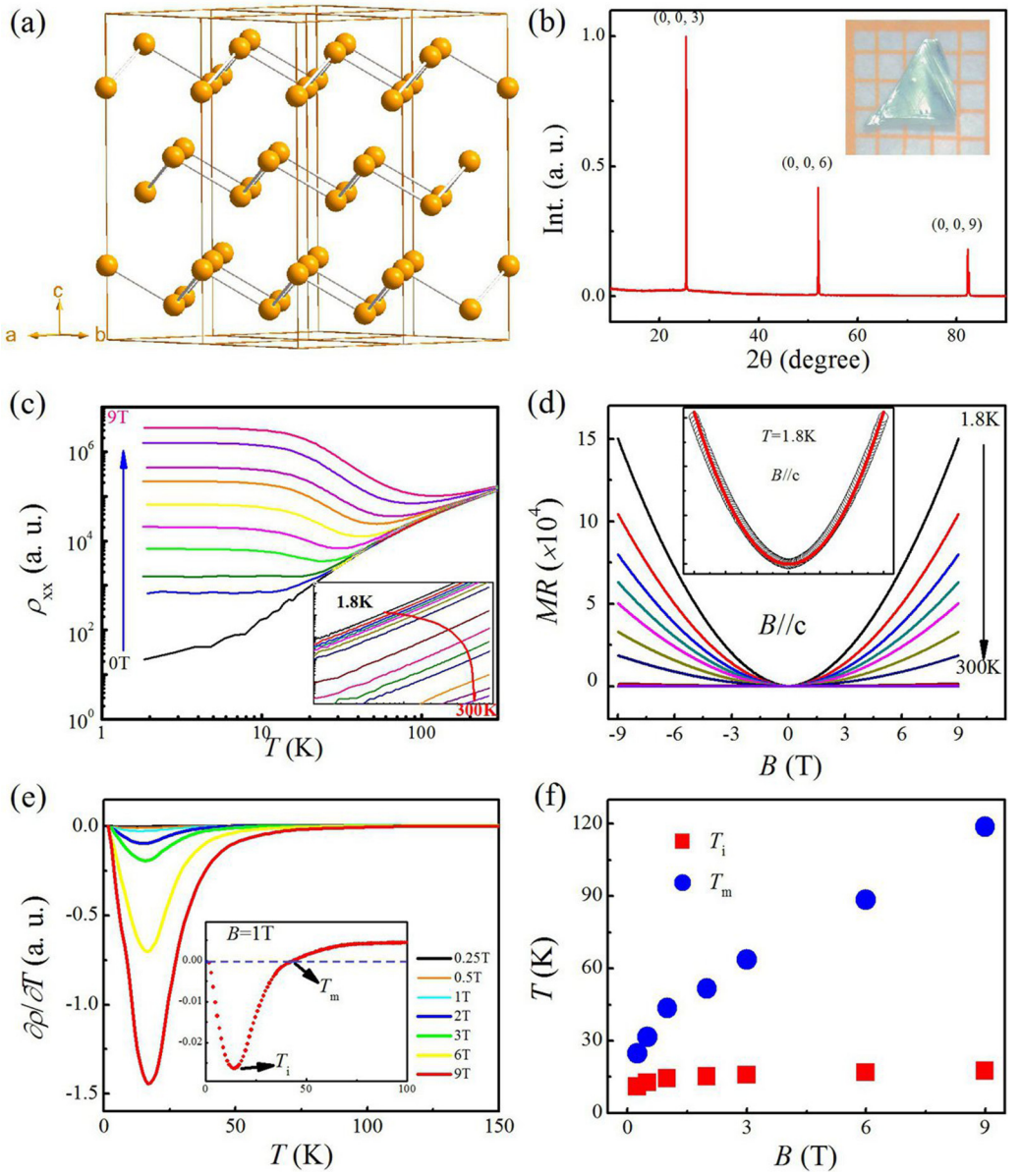

FIG. 1. (a) The crystal structure of α-As with $R\bar{3}m$ space group. (b) XRD pattern of α-As single crystal showing only (00l) reflections. (c) Temperature dependence of ρ_{xx} under selected magnetic fields on log-log scale for sample 1. At low temperatures, ρ_{xx} (B) curves show the same character: After an initial rapid rise, ρ_{xx} tends to saturate with a more distinct plateau. Inset: Plots of MR versus B on logarithmic scales. (d) Magnetic field-dependent MR at various temperatures. Inset: The solid line shows the quadratic fit to the MR data at 1.8 K. (e) The derivative $\partial\rho/\partial T$ curves taken at several magnetic fields. Inset: T_m and T_i are determined as the temperatures at which the $\partial\rho/\partial T$ versus T curves change sign and take a minimum. (f) Field dependence of T_m and T_i.

system characterized by a trigonal c direction, as shown in Fig. 1(b). The inset shows a photograph of a piece of cleaved crystal.

The magnetotransport measurements were performed with the four-probe method in a Quantum Design PPMS, and the electric current flows in the binary-bisectrix plane. For MR (or Hall resistivity) measurements, any Hall (or resistive) voltages due to misalignment of the voltage leads could be corrected by reversing the direction of the magnetic field. In order to achieve a uniform current distribution and to avoid the current jetting effect, the samples were cut in the rectangular specimens with a length of 3 mm, a width of 0.2 mm, and a thickness of 0.1 mm. The current leads were prepared by painting silver paste over the whole front and end surfaces of the specimens. The band structure is calculated by a first-principles calculation program package, the Vienna *ab initio* simulation package (VASP), and the exchange-correlation potential is the generalized gradient approximation (GGA) of Perdew-Burke-Ernzerhof (PBE) type.

The electrical resistivity was first measured along the bisectrix axis with the magnetic field applied normal to the binary-bisectrix plane. As shown in Fig. 1(c), at zero field, ρ_{xx} exhibits good metallic behavior with a large residual resistivity ratio [RRR $= \rho(300\,\mathrm{K})/\rho(2\,\mathrm{K})$] up to 6500 (in Ref. [17], the

RRR was reported up to ~9000), implying the high quality of the sample. With the application of magnetic fields, ρ_{xx} is enhanced drastically at low temperatures and shows a minimum, indicating that this system undergoes a field induced metal-to-insulator–like transition. Remarkably, ρ_{xx} saturates at very low temperatures, and leads to a resistivity plateau. To get a more clear view of the exotic transport behavior, we plotted the derivative $\partial\rho/\partial T$ curves at several magnetic fields in Fig. 1(e), where T_m and T_i are determined as the temperatures at which $\partial\rho/\partial T$ versus T curves change sign and take a minimum, which correspond to the temperatures of the emergence of metal-to-insulator–like transition and resistivity plateau in ρ_{xx} curves. As shown in Fig. 1(f), with the magnetic field increasing, T_m shifts to high temperature, while the applied field is seen to have little influence on T_i. The magnetic field induced metal-to-insulator–like transition and resistivity plateaus have also been observed in WTe_2 [4], Cd_3As_2 [5], TaAs [7], and other semimetals [18], in which the extremely large MR detected at low temperatures was ascribed to their own unique characteristics; the lack of inversion symmetry, linear band dispersion, perfect electron-hole compensation, and quasi-two-dimensional (2D) Fermi surfaces, respectively. The resistivity plateaus also seem to have their topological origin, similar to those observed in TIs such as Bi_2Te_2Se and SmB_6, where the protected metallic surface conductance dominates at low temperature [19,20].

In this material, the anomalous increase of ρ_{xx} (T) with decreasing temperature under high magnetic fields also results in an unexpectedly huge MR, as large as 15 000 000% at $T = 1.8$ K and $B = 9$ T. Figure 1(d) shows the magnetic field dependence of MR at various temperatures for field perpendicular to current. The MR increases quadratically with increasing the field over all the measured temperature range, which can be seen more clearly when the MR versus B is plotted on a logarithmic scale, as shown in the inset of Fig. 1(c). The log-log plot brings out the nice straight lines, which indicate that the MR of α-As follows the Kohler's rule in the temperature and field range measured, and the MR can be described in terms of semiclassical transport theory [21]. Interestingly, it should be noted that this behavior is in sharp contrast to that observed in the semimetal bismuth, in which the MR deviates from the quadratic field dependence, and eventually saturates at sufficiently high fields [22,23].

In the semiclassical two-band model [24], the magnetoresistivity ρ_{xx} and Hall resistivity ρ_{xy} can be expressed as the following equations:

$$\rho_{xx} = \frac{(n_h\mu_h + n_e\mu_e) + \mu_e\mu_h(n_h\mu_e + n_e\mu_h)B^2}{(n_h\mu_h + n_e\mu_e)^2 + \mu_e^2\,\mu_h^2\,(n_h - n_e)^2B^2}\frac{1}{e}, \quad (1)$$

$$\rho_{xy} = \frac{\left(n_h\mu_h^2 - n_e\mu_e^2\right) + \mu_e^2\,\mu_h^2\,(n_h - n_e)B^2}{(n_h\mu_h + n_e\mu_e)^2 + \mu_e^2\,\mu_h^2\,(n_h - n_e)^2B^2}\frac{B}{e}, \quad (2)$$

where n_e (or n_h) is the carrier density of the electron (or hole), $\mu_e(\mu_h)$ is the mobility of the electron (hole), respectively. In the case of perfect ($n_e = n_h$) or nearly perfect $(n_e\mu_e + n_h\mu_h)^2 \gg (n_e - n_h)^2(\mu_e\mu_h)^2B^2$ charge compensation, the MR $= \frac{\rho_{xx}(B)-\rho_{xx}(0)}{\rho_{xx}(0)} \approx \mu_e\mu_h B^2$ increases quadratically with the strength of magnetic field B without saturation, while the behavior of ρ_{xy} is more complex, which depends

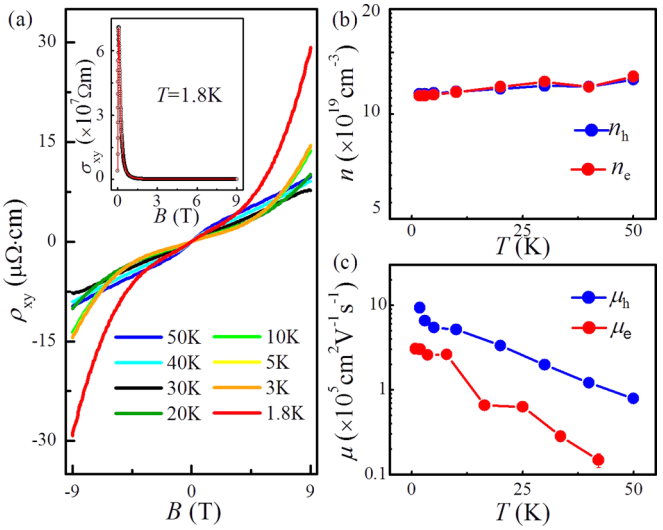

FIG. 2. (a) Hall resistivity ρ_{xy} measured at several temperatures from 1.8 to 50 K. Inset: Magnetic field dependence of σ_{xy} at 1.8 K. The solid line shows the best fitting with two-carrier model. (b) Temperature dependence of carrier density n_e and n_h. (c) Temperature dependence of carrier mobility μ_e and μ_h deduced by two-carrier model.

sensitively on the relative values of n_e, n_h, μ_e, and μ_h. Generally, a nonlinear field dependence of ρ_{xy} indicates the existence of carriers with different mobilities [25] or different polarities [7]. In this case, as shown in Fig. 2(a), ρ_{xy} (B) is positive with an upward curvature at low temperatures, and a downward curvature at high temperatures, which indicates clearly α-As has the multiple band character and the holelike carriers dominate its electrical transport behavior. For $T = 1.8$ K, the best fitted results using the two-band model are shown by the red curve in the inset of Fig. 2(a), which yield mobilities of $\mu_e \approx 2.4 \times 10^5\,\mathrm{cm^2\,V^{-1}\,s^{-1}}$ and $\mu_h \approx 9.35 \times 10^5\,\mathrm{cm^2\,V^{-1}\,s^{-1}}$ with corresponding carrier densities of $n_e = 1.13 \times 10^{20}\,\mathrm{cm^{-3}}$ (electron) and $n_h = 1.14 \times 10^{20}\,\mathrm{cm^{-3}}$ (hole), respectively. The carrier densities are close to those estimated from the previous dHvA measurements [12]. The very small difference between n_e and n_h demonstrates clearly that electron-hole compensation is close to perfect, and the variation of resistivity in transverse magnetic field significantly depends on extremely high hole mobilities. A similar behavior of ρ_{xx} and ρ_{xy} was also found in other samples with different residual resistivity ratio RRR. However, the magnitude of MR and carrier mobilities appears to be extremely sensitive to the sample quality. In particular, the MR shows a quadratic dependence on RRR (not shown here), as reported in newly discovered Weyl semimetals WTe_2 [26]. Here the excellent agreement between the measurements and simulation both for magnetoresistivity ρ_{xx} and Hall resistivity ρ_{xy} achieved by the semiclassical two-band model analysis indicates strongly that the huge magnetoresistance detected in gray arsenic stems from the nearly perfect electron-hole charge compensation and very high carrier mobilities.

Quantum oscillations in magnetic fields can provide a unique opportunity to gain insight into the nature of the Fermi surface topology. Experimentally, the oscillatory part of the

magnetoresistance ΔR_{xx}, i.e., the SdH oscillations, can be expressed in the following form [27–29]:

$$\Delta R_{xx} = R(T,B)\cos[2\pi(F/B - \lambda + \delta)], \tag{3}$$

where $\lambda = \frac{1}{2} - \frac{\varphi_B}{2\pi}$ is the Onsager phase factor taking the value $\lambda = 0, 1$ (or $\lambda = 1/2$) for the nontrivial (trivial) Berry phase φ_B. δ is a phase offset, with the value of $\delta = 0$ (or $\pm\frac{1}{8}$) for the 2D (or 3D) system. F is the oscillation frequency, which is proportional to the extremal cross section, $A_{\rm FS}$, of the Fermi surface; $F = (\hbar/2\pi e)A_{\rm FS}$ [30]. In this measurement, the SdH oscillations are smeared out by the extremely large MR background, as seen in Fig. 1(d). However, we can still extract the quantum oscillations by subtracting a polynomial fit to the background, as shown in Fig. 3(a). The oscillatory spectrum becomes more complex when the magnetic field is tilted from the trigonal axis, indicating the existence of multiple Fermi surfaces in this system. This can be seen more clearly by the fast Fourier transform (FFT) analysis as shown in Fig. 3(b). For

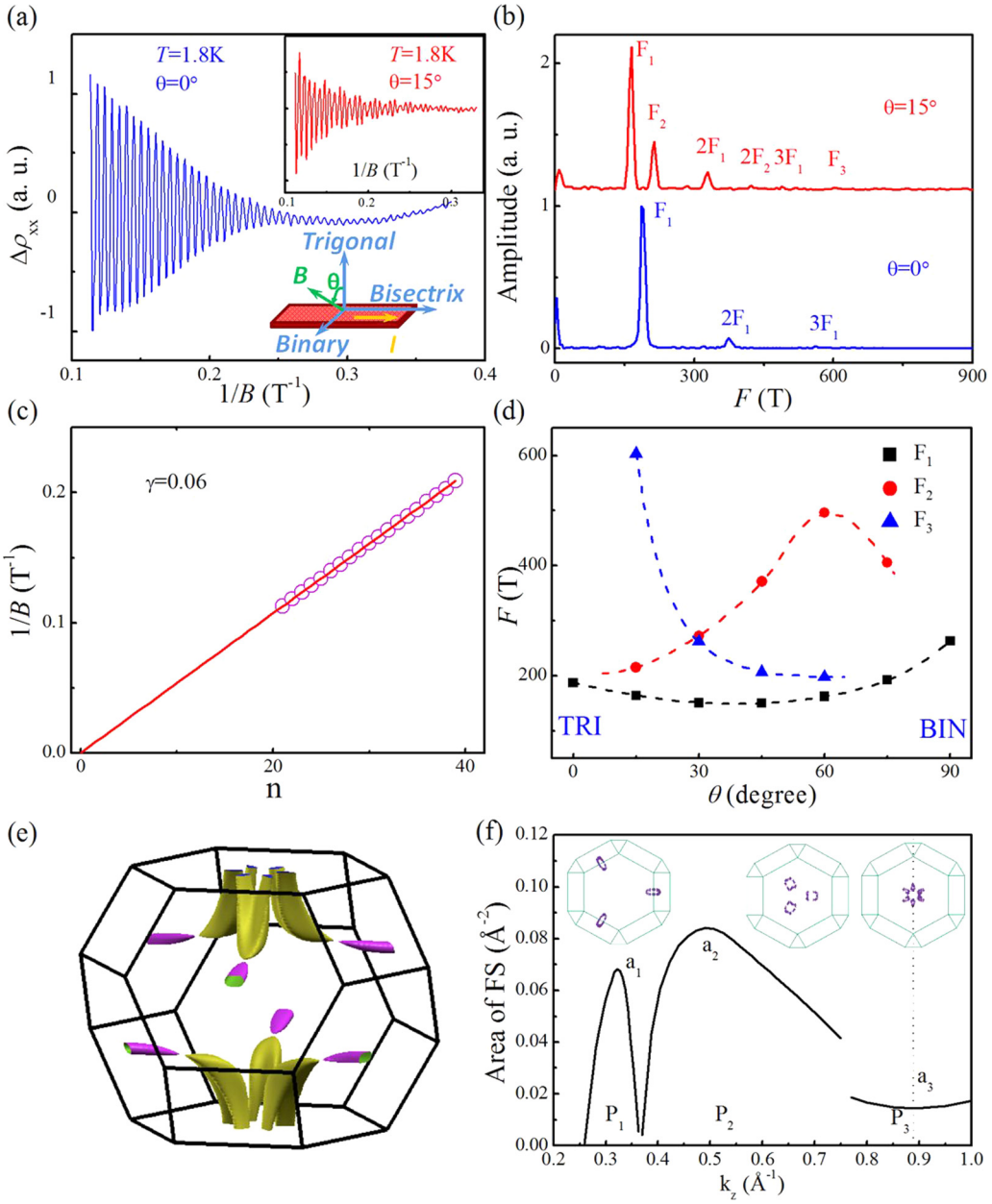

FIG. 3. (a) SdH oscillations in MR with the field applying along the trigonal axis at $T = 1.8$ K. Upper inset: SdH oscillations in MR obtained by rotating the field away from the trigonal axis with angle of 15°. Lower inset: the corresponding measurement configurations. (b) The FFT spectra of the SdH oscillations. (c) Landau level index plots $1/B$ versus n for the oscillation frequency of 187 T ($\theta = 0°$). The purple circles are the maxima of the resistance and the red line is the linear fit. The initial Landau level only reaches to $n = 21$ in a magnetic field up to 9 T, far away from the quantum limit. Higher-magnetic-field experiments will be useful to approach the quantum limit to further confirm the existence of the nontrivial Berry phase. (d) Angular dependence of the SdH frequencies. The dashed lines are guides for the eyes. (e) The calculated FS topology. (f) The relationship between k_z and the area of FS cut which is parallel to $k_x k_y$ surface. The origin is the central point of the Brillouin zone (BZ), and the dotted line demonstrates the edge of BZ.

the field directed along the trigonal axis, only one fundamental frequency and associated harmonics are observed. As the field is rotated away from the trigonal axis with an angle of 15°, three fundamental frequencies and associated harmonics are detected. The angular dependence of the SdH frequencies are plotted in Fig. 3(d) for rotation around [001], which is consistent with that observed in a previous dHvA study [12].

In our previous work, density functional theory (DFT) calculations were performed on α-As to illustrate the topological properties of the electronic structure [15]. It shows that, in the absence of spin-orbital coupling (SOC), there is a band crossing near the Fermi level, and the band crossings in the whole Brillouin zone (BZ) form a closed nodal line. When the SOC is further considered, an energy gap is opened along the node-line circle. Figure 3(e) shows the FS topology calculated with SOC. The FS of α-As mainly consists of three approximately ellipsoidal electron pockets and one multiply connected hole pocket. We find that the observed FS topology is in good agreement with the calculated ones in terms of the character of each sheet, indicating that the observed SdH oscillations in α-As originate mostly from the bulk state.

As mentioned above, the SdH effect can also probe the Berry phase. It is well known that the Berry phase associated with the Dirac cone is π in topological Dirac

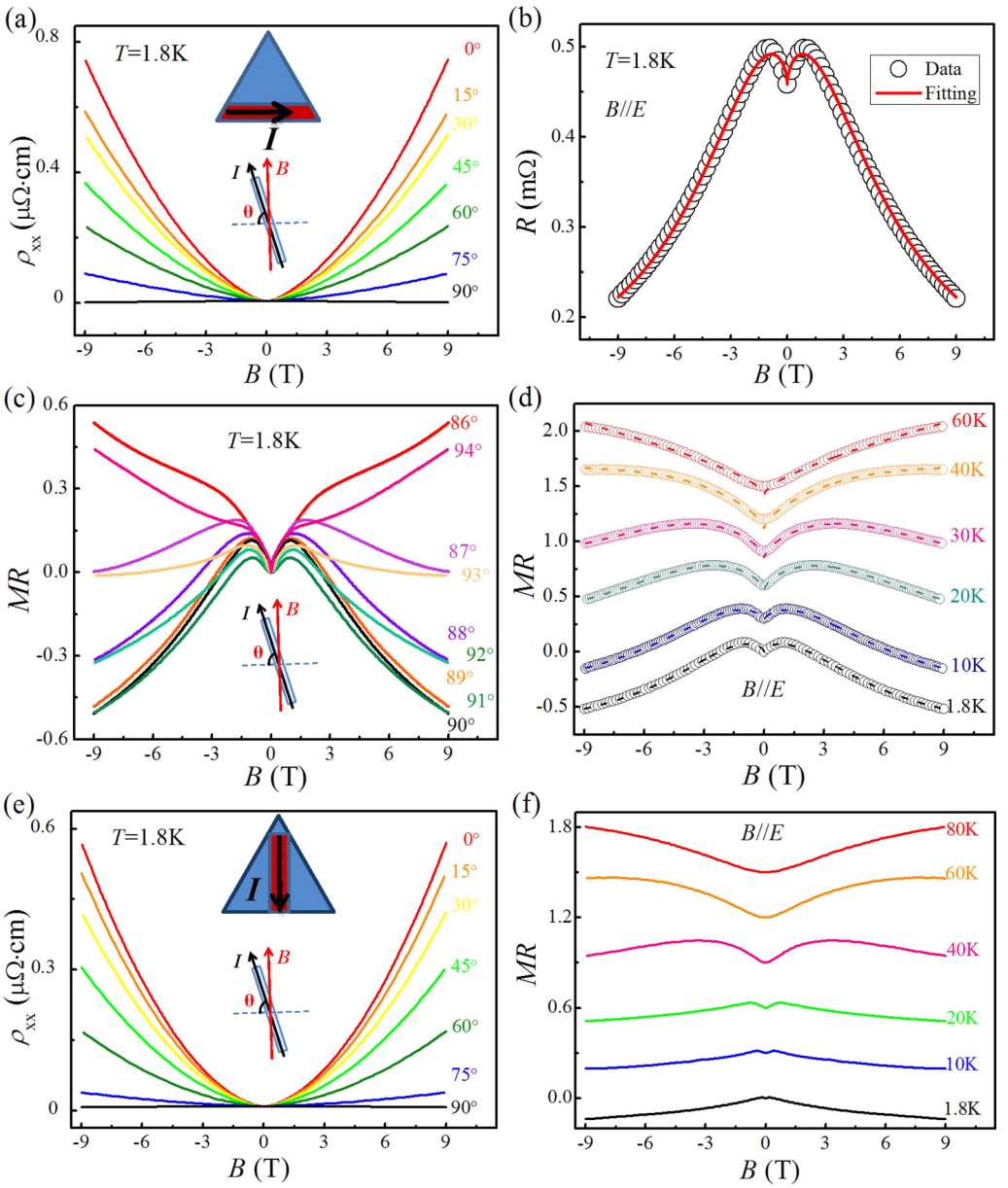

FIG. 4. (a) Magnetoresistivity with rotating field from perpendicular ($\theta = 0°$) to parallel ($\theta = 90°$) to the electric current at 1.8 K (sample 2; the electric current flows along the bisectrix axis). The insets depict the corresponding measurement configurations. (b) The negative MR at $\theta = 90°$ (open circles) and fitting curve (red solid line) at 1.8 K for sample 2. (c) Magnetoresistance measured in different rotating angles around $\theta = 90°$ for sample 2. The negative MR appeared at a narrow region around $\theta = 90°$, most obviously when ***B*//*I***. (d) The MR data at $\theta = 90°$ (open circles) and fitting curves (dashed lines) at various temperatures for sample 2. (e) Magnetoresistivity with rotating field from perpendicular ($\theta = 0°$) to parallel ($\theta = 90°$) to the electric current at 1.8 K (sample 3; the electric current flows along the binary direction). The insets depict the corresponding measurement configurations. (f) The longitudinal MR measured at various temperatures for sample 3.

materials [7,31,32]. In order to examine the Berry phase of α-As, we plotted the Landau level index n as a function of the peak and valley position ($1/B$) of the SdH oscillations ($\theta = 0^\circ$), as shown in Fig. 3(c), in which the oscillations are dominated by the fundamental frequency $F_\alpha = 187\,\mathrm{T}$. The linear extrapolation of the plot yields the value of $\lambda - \delta$ to be ~0.06, indicating the presence of nontrivial π Berry phase in α-As. Data collected from several different samples are also analyzed to further confirm the existence of the nontrivial Berry phases in α-As, which gives a strong signature of π Berry phase arising from 3D Dirac electrons.

The change of resistance of α-As by tilting the magnetic field from perpendicular ($\theta = 0^\circ$) to parallel ($\theta = 90^\circ$) to the direction of the current has also been investigated, as shown in Fig. 4(a). The inset illustrates the configuration of the measurements, where $\boldsymbol{B}$ is rotated always within the binary-bisectrix plane, and the sample 2 with RRR~200 was cut along the bisectrix axis. We find that the giant MR strongly depends on θ and decreases considerably with θ increasing. When the magnetic field is rotated to be parallel to the electric current ($\theta = 90^\circ$, $\boldsymbol{B}//I$), we get a negative MR with a value of -50% at 1.8 K and $B = 9\,\mathrm{T}$. The sharp dip around zero fields may be attributed to the weak antilocalization effect (WAL), which is observed commonly in graphene and TIs [33–35], in which Dirac fermions dominate the magnetoelectric transport. We also found the negative longitudinal MR and WAL disappeared rapidly when the sample was warmed up to 40 K; see Fig. 4(d).

To further identify the character of the observed negative longitudinal MR, we fit the data using a semiclassical formula [7] in the magnetic field $-9\,\mathrm{T} \leqslant B \leqslant 9\,\mathrm{T}$:

$$\sigma(B) = (1 + C_W B^2)\sigma_{\mathrm{WAL}} + \sigma_N, \tag{4}$$

where

$$\sigma_{\mathrm{WAL}} = \sigma_0 + a\sqrt{B}, \tag{5}$$

and

$$\sigma_N^{-1} = \rho_0 + AB^2. \tag{6}$$

σ_0 is the zero field conductivity, and C_{W} is a positive parameter which originates from the topological $\boldsymbol{E}.\boldsymbol{B}$. Such a topological term will generate chiral current in the nonorthogonal magnetic and electric fields. σ_{WAL} and σ_N are those from WAL effect and conventional nonlinear band contributions around the Fermi level, respectively. The fittings show excellent agreement between the experimental data and theoretical curves with the parameters of $\sigma_0 = 2.87 \times 10^6\,\Omega^{-1}\,\mathrm{cm}^{-1}$, $a = -5.76 \times 10^7\,\Omega^{-1}\,\mathrm{m}^{-1}\,\mathrm{T}^{-0.5}$, $C_W = 0.095\,\mathrm{T}^{-2}$, $A = 2.48 \times 10^{-9}\,\Omega\,\mathrm{cm}\,\mathrm{T}^{-2}$, and $\rho_0 = 3.58 \times 10^{-7}\,\Omega\,\mathrm{cm}$ at $T = 1.8\,\mathrm{K}$. It seems to suggest that α-As has a signature of Dirac fermions' characters as detected in other topological semimetals [6,7].

Remarkably, we find that the negative MR is sensitive to deviations of $\boldsymbol{B}$ from $\boldsymbol{E}$, rather than being pinned to a special crystal axis, similar to that of Dirac semimetal Na_3Bi [6]. As shown in Figs. 4(e) and 4(f), the measurement was performed on sample 3 cut from the same large piece as sample 2, but the electric current flows along the binary direction. When the magnetic field $\boldsymbol{B}$ is tilted from perpendicular to parallel $\boldsymbol{E}$ within a binary-bisectrix plane, the MR decreases gradually and leads also to the emergence of negative MR for $\theta = 90^\circ$.

Recently the negative MR under parallel electric and magnetic fields has been found not only in Dirac or Weyl semimetals, [6,7] where the gap vanishes at some k points, but also in some material systems, where a small energy gap does exist throughout the whole BZ [36]. This implies that the contribution from chiral anomaly may persist when the coupling between two Weyl points with opposite chirality is not big enough. Since the dc resistivity is mainly contributed by the states near the Fermi level, opening a small gap away from the Fermi level should not kill the effect immediately. In α-As single crystal, as found by both DFT calculation and ARPES measurement, the minimum direct band gap between the valence and conduction bands is about 0.1 eV, which is comparable to the Fermi energy 5.49 eV. Why the negative MR can survive in this situation is still an interesting and important question, which may relate to the long mean free path in α-As crystal.

In summary, the magnetotransport properties of α-As single crystal have been studied in detail. We find that α-As exhibits an extremely large quadratic field-dependent magnetoresistance. Based on the semiclassical two-band model, these exotic magnetotransport behaviors can be well understood with the electron-hole compensation mechanism. Further analysis of the SdH oscillations gives a nontrivial π Berry phase. Remarkably, in the presence of parallel magnetic and electric fields, a weak antilocalization (WAL) effect and a pronounced negative longitudinal MR are observed. Our magnetotransport data seem to indicate that α-As has a strong signature of Dirac fermions' characters as detected in other topological semimetals, in contrast to the results of first-principles calculations and ARPES measurement. Systematical studies on such a simple element of VA not only shed new light on the understanding of the extremely large magnetoresistance and anomalous magnetotransport properties, but also promote its potential applications in electronic devices.

This work was supported by National Basic Research Program of China 973 Program (Grant No. 2015CB921303), National Key Research Program of China (Grant No. 2016YFA0300604), and the "Strategic Priority Research Program (B)" of the Chinese Academy of Sciences (Grant No. XDB07020100).

L.Z. and Q.X. contributed equally to this work.

[1] M. N. Baibich, J. M. Broto, A. Fert, F. Nguyen Van Dau, F. Petroff, P. Etienne, G. Creuzet, A. Friederich, and J. Chazelas, Phys. Rev. Lett. **61**, 2472 (1988).

[2] A. P. Ramirez, J. Phys.: Condens. Matter **9**, 8171 (1997).

[3] Y. Moritomo, A. Asamitsu, H. Kuwahara, and Y. Tokura, Nature **380**, 141 (1996).

[4] M. N. Ali, J. Xiong, S. Flynn, J. Tao, Q. D. Gibson, L. M. Schoop, T. Liang, N. Haldolaarachchige, M. Hirschberger, N. P. Ong, and R. J. Cava, Nature **514**, 205 (2014).

[5] T. Liang, Q. Gibson, Mazhar N. Ali, M. H. Liu, R. J. Cava, and N. P. Ong, Nat. Mater. **14**, 280 (2015).

[6] J. Xiong, S. K. Kushwaha, T. Liang, J. W. Krizan, M. Hirschberger, W. Wang, R. J. Cava, and N. P. Ong, Science **350**, 413 (2015).
[7] X. C. Huang, L. X. Zhao, Y. J. Long, P. P. Wang, D. Chen, Z. H. Yang, H. Liang, M. Q. Xue, H. M. Weng, Z. Fang, X. Dai, and G. F. Chen, Phys. Rev. X **5**, 031023 (2015).
[8] D. Schiferl and C. S. Barrett, J. Appl. Crystallogr. **2**, 30 (1969).
[9] Z. Zhu, J. Guan, and D. Tománek, Phys. Rev. B **91**, 161404(R) (2015).
[10] J. Vanderkooy and W. R. Datars, Phys. Rev. **156**, 671 (1967).
[11] C. Miziumski and A. W. Lawson, Phys. Rev. **180**, 749 (1967).
[12] M. G. Priestley, L. R. Windmiller, J. B. Ketterson, and Y. Eckstein, Phys. Rev. **154**, 671 (1967).
[13] J. Vanderkooy and W. R. Datars, Can. J. Phys. **46**, 1935 (1968).
[14] A. P. Jeavons and G. A. Saunders, Proc. R. Soc. London, Ser. A **310**, 415 (1969).
[15] P. Zhang, J. Z. Ma, Y. Ishida, L.-X. Zhao, Q.-N. Xu, B.-Q. Lv, K. Yaji, G.-F. Chen, H.-M. Weng, X. Dai, Z. Fang, X.-Q. Chen, L. Fu, T. Qian, H. Ding, and S. Shin, Phys. Rev. Lett. **118**, 046802 (2017).
[16] C. Uher, J. Cryst. Growth **62**, 141 (1983).
[17] C. Uher and D. T. Morellif, J. Phys. F: Met. Phys. **16**, L103 (1986).
[18] F. F. Tafti, Q. D. Gibson, S. K. Kushwaha, N. Haldolaarachchige, and R. J. Cava, Nat. Phys. **12**, 272 (2016).
[19] D. J. Kim, J. Xia, and Z. Fisk, Nat. Mater. **13**, 466 (2014).
[20] Z. Ren, A. A. Taskin, S. Sasaki, K. Segawa, and Y. Ando, Phys. Rev. B **82**, 241306 (2010).
[21] A. B. Pippard, *Magnetoresistance in Metals* (Cambridge University Press, Cambridge, 1989).
[22] B. Fauqué, B. Vignolle, C. Proust, J. P. Issi, and K. Behnia, New J. Phys. **11**, 113012 (2009).
[23] Y. Kopelevich, J. H. S. Torres, R. R. da Silva, F. Mrowka, H. Kempa, and P. Esquinazi, Phys. Rev. Lett. **90**, 156402 (2003).
[24] N. W. Ashcroft and N. D. Mermin, *Solid State Physics* (Holt, Rinehart and Winston, New York, 1976).
[25] L. X. Zhao, X. C. Huang, Y. J. Long, D. Chen, H. Liang, Z. H. Yang, M. Q. Xue, Z. A. Ren, H. M. Weng, Z. Fang, X. Dai, and G. F. Chen, arXiv:1512.07360.
[26] M. N. Ali, L. Schoop, J. Xiong, S. Flynn, Q. Gibson, M. Hirschberger, N. P. Ong, and R. J. Cava, Europhys. Lett. **110**, 67002 (2015).
[27] G. P. Mikitik and Yu. V. Sharlai, Phys. Rev. Lett. **82**, 2147 (1999).
[28] H. Murakawa, M. S. Bahramy, M. Tokunaga, Y. Kohama, C. Bell, Y. Kaneko, N. Nagaosa, H. Y. Hwang, and Y. Tokura, Science **342**, 1490 (2013).
[29] E. N. Adams and T. D. Holstein, J. Phys. Chem. Solids **10**, 254 (1959).
[30] D. Shoenberg, *Magnetic Oscillations in Metals* (Cambridge University Press, Cambridge, England, 1984).
[31] L. P. He, X. C. Hong, J. K. Dong, J. Pan, Z. Zhang, J. Zhang, and S. Y. Li, Phys. Rev. Lett. **113**, 246402 (2014).
[32] Y. Zhang, Y. W. Tan, H. L. Stormer, and P. Kim, Nature, **438**, 201 (2005).
[33] X. S. Wu, X. B. Li, Z. M. Song, C. Berger, and W. A. de Heer, Phys. Rev. Lett. **98**, 136801 (2007).
[34] M. H. Liu, J. S. Zhang, C. Z. Chang, Z. C. Zhang, X. Feng, K. Li, K. He, L. L. Wang, X. Chen, X. Dai, Z. Fang, Q. K. Xue, X. C. Ma, and Y. Y. Wang, Phys. Rev. Lett. **108**, 036805 (2012).
[35] S. Ishiwata, Y. Shiomi, J. S. Lee, M. S. Bahramy, T. Suzuki, M. Uchida, R. Arita, Y. Taguchi, and Y. Tokura, Nat. Mater. **12**, 512 (2013).
[36] Q. Li, D. E. Kharzeev, C. Zhang, Y. Huang, I. Pletikosić, A. V. Fedorov, R. D. Zhong, J. A. Schneeloch, G. D. Gu, and T. Valla, Nat. Phys. **12**, 550 (2016).